

Kinematics, turbulence and evolution of planetary nebulae ^{*}

Krzysztof Gesicki,¹ Agnes Acker,² and Albert A. Zijlstra³

¹ Centrum Astronomii UMK, ul. Gagarina 11, PL-87-100 Torun, Poland
e-mail: Krzysztof.Gesicki@astri.uni.torun.pl

² Observatoire astronomique de Strasbourg, 11 rue de l'Université, 67000 Strasbourg, France
e-mail: acker@astro.u-strasbg.fr

³ Astrophysics Group, Physics Department, UMIST, PO Box 88, Manchester M60 1QD, United Kingdom
e-mail: a.zijlstra@umist.ac.uk

Received 23 October 2002 / Accepted 6 January 2003

Abstract.

This paper discusses the location of a sample of planetary nebulae on the HR diagram. We determine the internal velocity fields of 14 planetary nebulae from high-resolution echelle spectroscopy, with the help of photoionization models. The mass averaged velocity is shown to be a robust, simple parameter describing the outflow. The expansion velocity and radius are used to define the dynamical age; together with the stellar temperature, this gives a measurement of the luminosity and core mass of the central star. The same technique is applied to other planetary nebulae with previously measured expansion velocities, giving a total sample of 73 objects. The objects cluster closely around the Schönberner track of $0.61 M_{\odot}$, with a very narrow distribution of core masses. The masses are higher than found for local white dwarfs. The luminosities determined in this way tend to be higher by a factor of a few than those derived from the nebular luminosities. The discrepancy is highest for the hottest (most evolved) stars. We suggest photon leakage as the likely cause. The innermost regions of the non-[WC] nebulae tend to show strong acceleration. Together with the acceleration at the ionization front, the velocity field becomes 'U'-shaped. The presence of strong turbulent motions in [WC] nebulae is confirmed. Except for this, we find that the [WC] stars evolve on the same tracks as non-[WC] stars.

Key words. Planetary nebulae: general – Stars: evolution – Stars: HR diagram

1. Introduction

The study of the expansion velocities of planetary nebulae (PN) has two goals. The first goal is to develop our understanding of the hydrodynamical evolution of the nebula. The importance of this is shown by Stasińska & Tylenda (1994), who compare theoretical evolutionary models with the planetary-nebula population of the Galactic Bulge. They show how the comparison of such models with observed properties of the PN population can be used to derive properties such as the mass distribution of the central stars. However, they comment on the lack of expansion velocity data, which is required to “strongly constrain the average properties of Galactic bulge PN and especially the masses of their central stars”.

The second goal is to characterize the parameters of the superwind and study its dependence on the progenitor's age and metallicity. It is expected that a dust-driven wind is less efficient at low metallicity, leading to heavier white dwarfs (e.g. Zijlstra 1999), but there is no observational confirmation of this. In fact white dwarf masses measured in (metal-poor) globular clusters (Richer et al. 1997) seem low compared to those

of central stars of Bulge planetary nebulae (Gesicki & Zijlstra 2000).

In the present paper we discuss a sample of PNe for which we have high-resolution spectra covering [O III], [N II] and H α , which allow us to model the velocity fields in some detail. In two cases is the 6560Å He II line used instead of [O III]. Using these lines which trace both the inner and outer regions, we find that the most common velocity profile is 'U'-shaped, with the highest velocities near the outer edge (as predicted by hydrodynamical models) and the inner edge (which is less expected). The mass-averaged expansion velocity is shown to be a well-defined and measurable parameter. This parameter allows us to accurately place the objects on the HR diagram.

2. The observations

The observations were performed at the ESO CAT telescope during 1993 and 1994. This was a subsidiary 1.4m telescope feeding into the CES spectrograph located at the neighbouring 3.6m telescope. The long camera was used giving a spectral resolution of 60 000 (corresponding to 5 km s^{-1}). The slit width was $2''$, and the CCD was binned to $2''$ pixels. The spectra used here use only the central row of pixels. (As the nebulae studied

^{*} Based on observations taken at the ESO

here are compact and the CAT was not an imaging-quality telescope, no spatial information was expected.) The spectrum covers one order of the echelle, including H α and the [N II] lines at 6548Å and 6853Å. This was combined with earlier published spectra of the [O III] 5007Å line, take with the same telescope but with a resolution of only 30 000.

We assume the nebulae to be spherically symmetric. This is partly necessitated by the data. The objects tend to be resolved by the instrumental setup (as shown by the line splitting which is often seen). But the CAT suffers from field rotation so that the orientation of the slit on the sky changes during the exposure, and may be different between the two separate setups. If the nebulae are not symmetric, the two spectral settings may trace regions in the nebula with different conditions.

For our modeling we will strictly assume spherical symmetry. *Assuming* symmetry does not *make* the nebula symmetric—the most common shape for PNe is in fact elliptical. In a previous paper (Gesicki & Zijlstra 2003) we discuss the effect of ellipticity on the data and models, using very compact (extragalactic) PNe for which integrated spectra could be obtained. We will comment on this problem below, when discussing the interpretation of the deduced velocity profiles.

3. Method of analysis

Recently in Gesicki & Zijlstra (2003) we published a very detailed description of the modelling procedure, therefore we provide only a short summary of the method.

The computer model first solves for the photo-ionization equilibrium, where we attempt to reproduce the observed line intensities. Once a satisfactory solution has been obtained, are the line profiles calculated and compared with the observations.

The nebula is approximated as a spherical shell described by the inner and outer radius, the total mass, the radial density distribution, the radial velocity field, and the chemical composition. As far as possible the values for the radii and chemical composition are taken from the literature. The star is assumed to be a black body with a luminosity and effective temperature. The temperature is again taken from the literature if possible, while the luminosity of the star is determined mainly by the H β flux, once a distance has been chosen.

Once the photoionization model is complete, we calculate the emissivity distribution for the ionic lines. The line profile can now be calculated, taking into account the slit aperture (which does not cover the full nebula) and the seeing (which scatters light rays outside the aperture into the slit). The velocity field is adjusted to fit the line profiles of all three lines simultaneously. O III and N II tend to cover the inner and outer regions of the nebula, respectively, while hydrogen is formed throughout the ionized nebula. This set is therefore the minimum required for a realistic description of the full nebula.

4. The nebulae

Spectra of 14 nebulae are analyzed in this paper. Twelve are located towards the Galactic Bulge (but only 7 are likely Bulge members), and two are in the Southern Galactic plane. The objects are specifically chosen as having [O III] observations

available. More objects were observed at the CAT in H α and [N II], but without [O III] the velocity field can be insufficiently constrained. There are however two objects where a He II line was detected next to H α , and these are included in the present paper as this line provides a good alternative to [O III].

We have previously analyzed a large set of nebulae using only the [O III] line (Gesicki & Zijlstra 2000). By necessity a simple, linear velocity field was used. The addition of other lines allows us to significantly improve on the earlier results.

The observed nebulae are listed in Table 1, together with some parameters obtained from the fit. The spectra, together with the fitted line profiles, are shown in Figs. 1–14.

4.1. Comments on individual nebulae

002.6+08.1 (H 1-1) This object, likely in the Bulge, is the only density bounded object in our sample: the evidence for this comes from the weakness of the [N II] (and [S II]) lines. The electron temperature is high. The inner radius is chosen as 0.3 (as opposed to the usual 0.4) times the outer radius, in order to fit the limited line splitting observed in [O III]. The fitted velocity field increases monotonically with radius, with the velocity minimum at the inner radius. Compared to the other nebulae analyzed here, this appears to be unusual. There is no evidence for a turbulent component in the velocity field, in spite of the wels-type (weak-emission-line star). The jump in the [N II] line profile at -20 km s^{-1} (Fig. 1) is believed to be an artifact of the data reduction process.

003.9–02.3 (M 1-35) The distance adopted for the fit is inconsistent with Bulge membership: at larger distances the ionized mass becomes rather high ($0.36 M_{\odot}$). A radio image is shown in Zijlstra et al. (1989), but the resolution is limited. There is some indication that the central peak is slightly shifted. The line profiles show some structure. There is a dip near the centre of H α which may be an instrumental problem. The [O III] line show a central peak which is absent in the [N II] line. This feature is not reproduced in the fit, but indicates excess high-excitation gas at or near systemic velocity. The best fit is shown in Fig.2, using a 'U'-shaped velocity field, where the minimum velocity is located at an intermediate radius (possibly near the half-mass radius).

006.1+08.3 (M 1-20) Schwarz et al. (1992) have published an image but it is difficult to measure a diameter from this. The high-resolution VLA radio image (Aaquist & Kwok 1990) shows a compact torus with very small inner radius ($0.25''$) and outer radius of roughly $0.8''$. In the perpendicular direction the outer radius is a little over $1''$. The image appears mildly bipolar. The fit uses an inner radius of $0.2 \times R_{\text{out}}$, as indicated by the radio image. The [O III] line is very narrow. The best fit therefore proposes almost stationary gas (1 km s^{-1}) at the inner radius. The expansion velocity increases rapidly further out.

278.1–05.9 (NGC 2867) This object contains a hot [WC] central star. We have no [O III] data but the He II 6560Å line is detected and provides an alternative. Schwarz et al. (1992) present an image showing a dense inner ring and a very large but much fainter halo. Our fit, and probably our data, only relate to the inner ring. The strong [N II] and [S II] suggest that

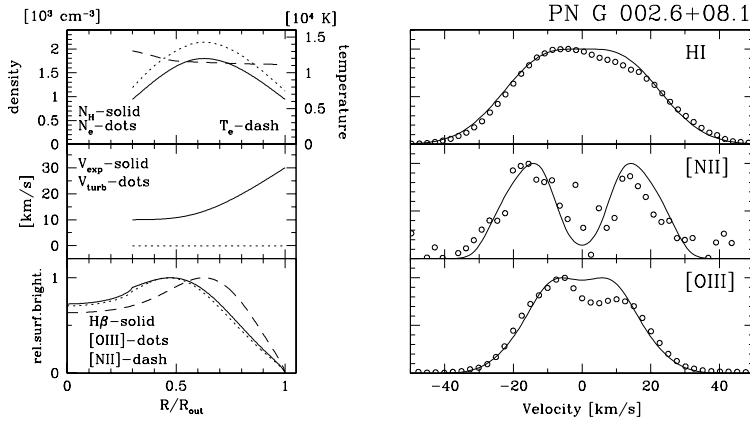


Fig. 1. The model results for the PN 002.6+08.1. The right panels show the fit (solid lines) against the observations (open circles) for all three lines. The top-left panel shows the density distribution (N_H and N_e) and the electron temperature. The middle-left panel shows the velocity field and the bottom-left panel shows the predicted surface brightness distribution (not including seeing) which could be compared against radial cuts through images.

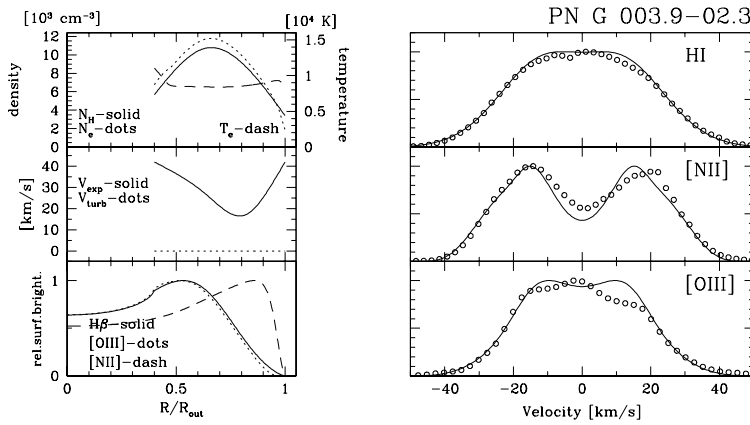


Fig. 2. As Fig. 1, for the PN 003.9-02.3.

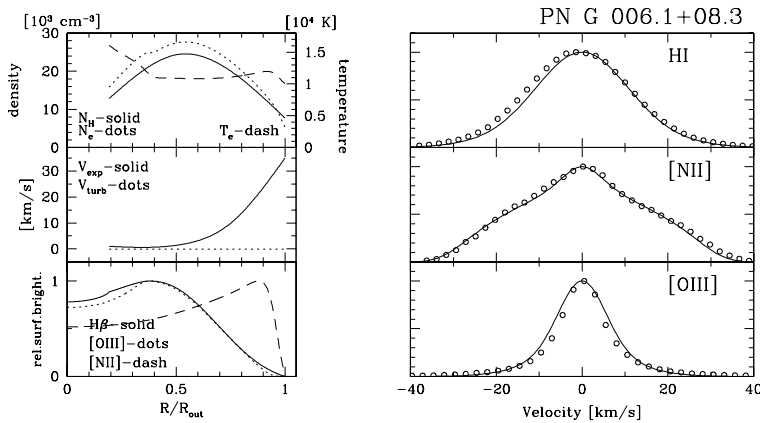


Fig. 3. As Fig. 1, for the PN 006.1+08.3

the inner ring is ionization bounded. This raises the question what ionizes the halo. The optical image suggests the ring is clumpy: photon leakage between the clumps could ionize the halo—or the halo may be recombining. The fit suggests considerable turbulence, as appears to be the rule for [WC] stars: e.g. Gesicki & Zijlstra (2003) for a discussion of a similar nebula.

In addition to the constant turbulence, the expansion velocity increases outward.

278.8+04.9 (PB 6) The photo-ionization model works poorly, as the observed He II 4686Å (Peña et al. 2001) is far stronger than the model predicts. However, the observed line may arise from the star which is a hot [WC] star. As in the pre-

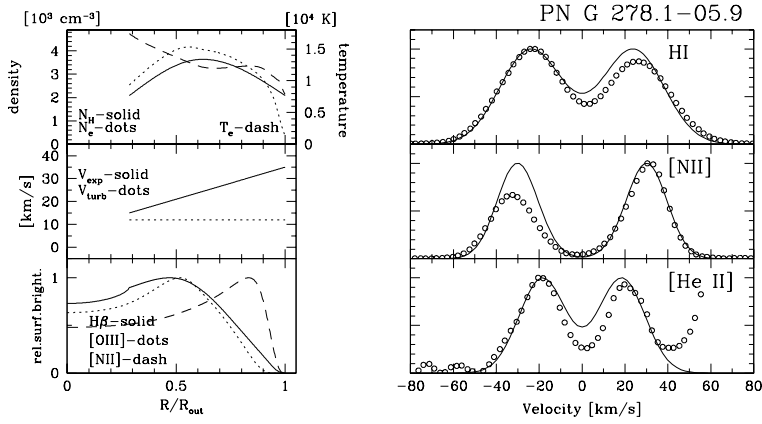


Fig. 4. As Fig. 1, for the PN 278.1-05.9

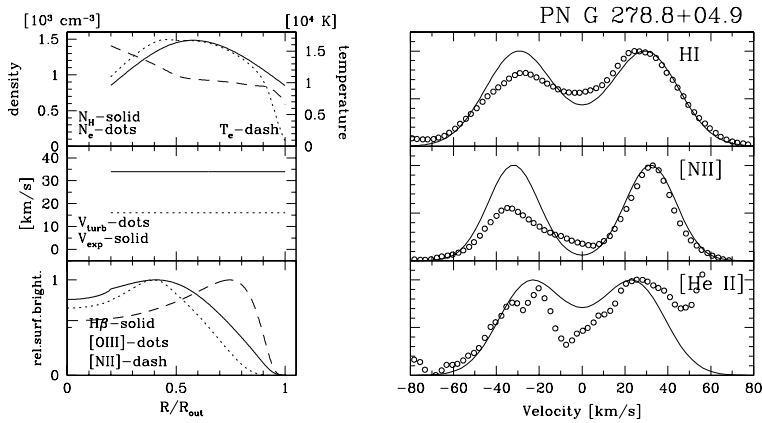


Fig. 5. As Fig. 1, for the PN 278.8+04.9

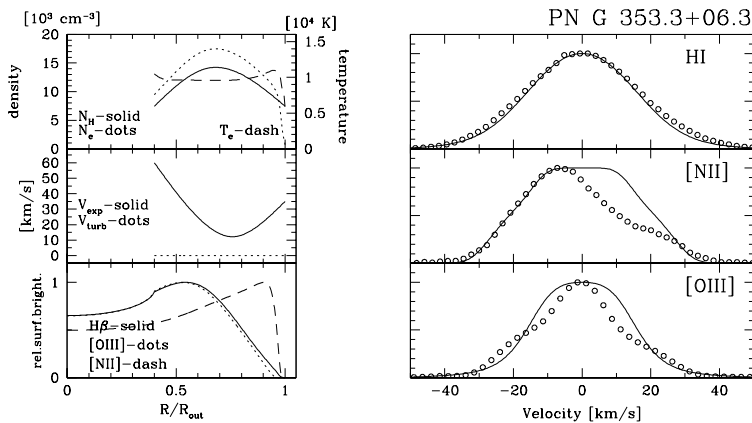


Fig. 6. As Fig. 1, for the PN 353.3+06.3.

vious object, the He II 6561Å was used instead of the [O III] line. A turbulent solution provides the best fit, with a constant but high expansion velocity.

353.3+06.3 (M 2-6) The [O III] line is very difficult to fit, with a narrow core but wide and strong wings. The [N II] is very asymmetric. We have assumed that this reflects line splitting where one component is very weak, but there may other interpretations. In fact the radio image (Gathier et al. 1983) is almost unresolved, as is the optical H α image of Bedding &

Zijlstra (1994), suggesting line splitting is less likely. The fit must be considered as uncertain. However, the extended wings of the [O III] line suggests high-velocity gas at or near the inner radius.

353.5-04.9 (H 1-36) The [O III] has very wide wings. The star is listed as a possible symbiotic (Acker et al. 1992). Aaquist & Kwok (1990) find the radio image to be unresolved, even with the VLA (high resolution) A-array. The line profiles of both H α and [O III] are asymmetric, with an extended red wing.

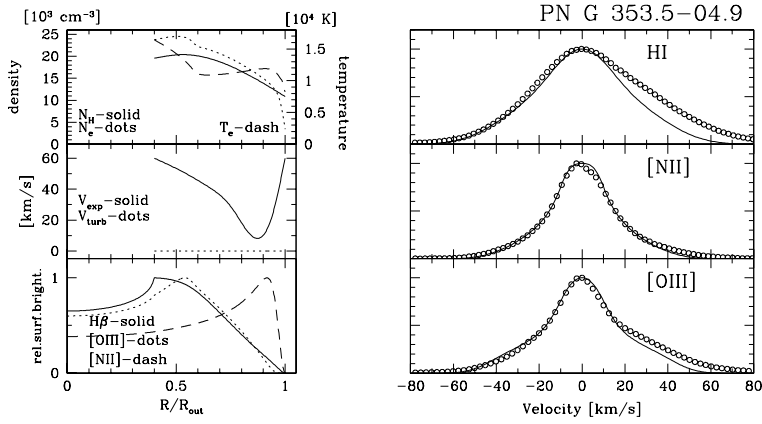


Fig. 7. As Fig. 1, for the PN 353.5-04.9.

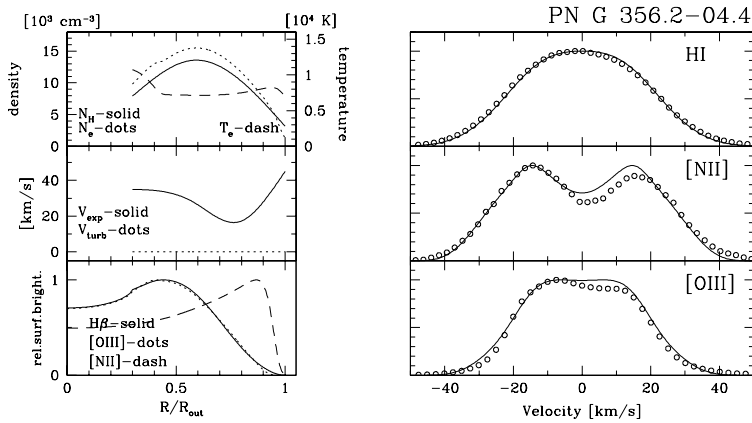


Fig. 8. As Fig. 1, for the PN 356.2-04.4

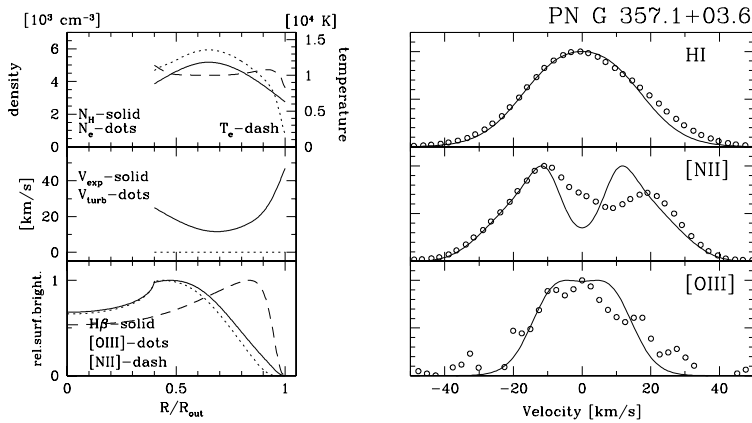


Fig. 9. As Fig. 1, for the PN 357.1+03.6

The compactness of the nebula indicates that this asymmetry is intrinsic to the nebula. A 'U'-shaped velocity profile is used, with velocity minimum close to the outer radius. The outermost density is also reduced to fit the rather narrow [N II] line.

356.2-04.4 (Cn 2-1) The $H\alpha$ image of this object is very compact (Bedding & Zijlstra 1994). But our spectra show significant splitting of the [N II] line, suggesting that the low excitation gas is more extended than the slit width of $2''$. The inner

radius was chosen as $0.3 \times R_{\text{out}}$, to avoid line splitting of [O III]. A good fit could be obtained with a 'U'-shaped velocity field.

357.1+03.6 (M 3-7) The [O III] line is weak and rather noisy which gives relatively poor constraints on the fit. The velocity of the inner region is therefore not well constrained. The [N II] line shows strong splitting whilst [O III] does not, but otherwise the line widths are similar. The [N II] profiles require a component at low velocity, but the [O III] is too wide for this component to solely dominate the inner nebula. We therefore

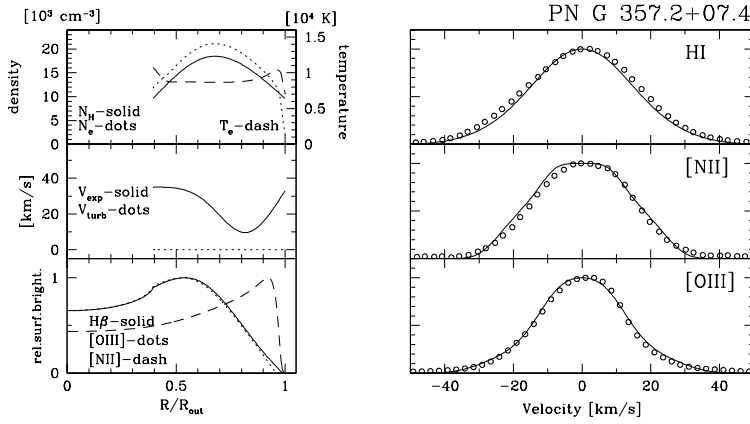


Fig. 10. As Fig. 1, for the PN 357.2+07.4

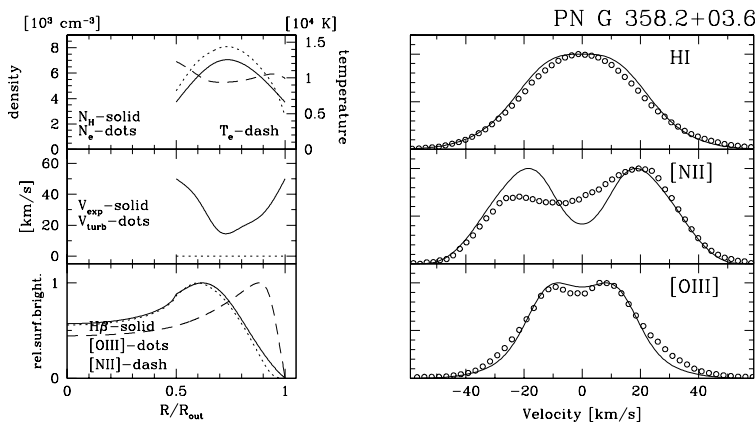


Fig. 11. As Fig. 1, for the PN 358.2+03.6

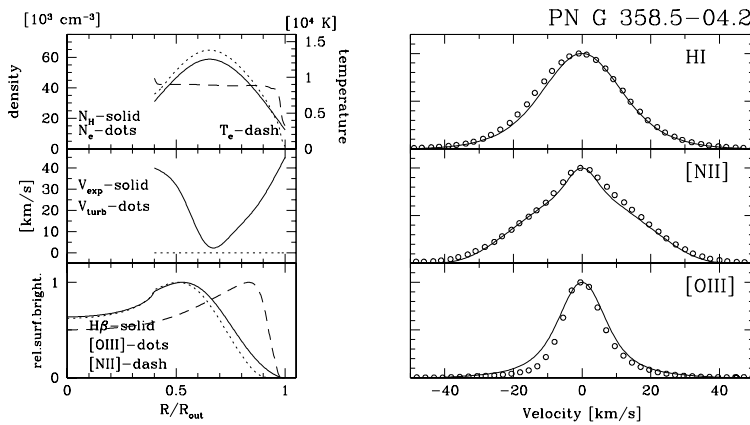


Fig. 12. As Fig. 1, for the PN 358.5-04.2

arrive at higher velocities near the inner and the outer edge and lower in-between. The poorly resolved image in Zijlstra et al. (1989) shows some indication for ellipticity.

357.2+07.4 (M 4-3) The lack of line splitting suggests an unresolved nebula, in agreement with the radio image (Gathier et al. 1983) and H α image (Bedding & Zijlstra 1994). The best fit uses a 'U'-shaped velocity field with the highest velocity at the inner edge. The H α line is a little too narrow in the adopted

fit, which may indicate that the electron temperature is underestimated.

358.2+03.6 (M 3-10) A 'U'-shaped velocity field is required with very high velocities (60 km s^{-1}) near the inner and outer edge. The high velocity gas is indicated by the wide wings seen in all three lines. The [OIII] line shows some splitting: to reproduce this, the inner radius was chosen as $0.5 \times R_{\text{out}}$.

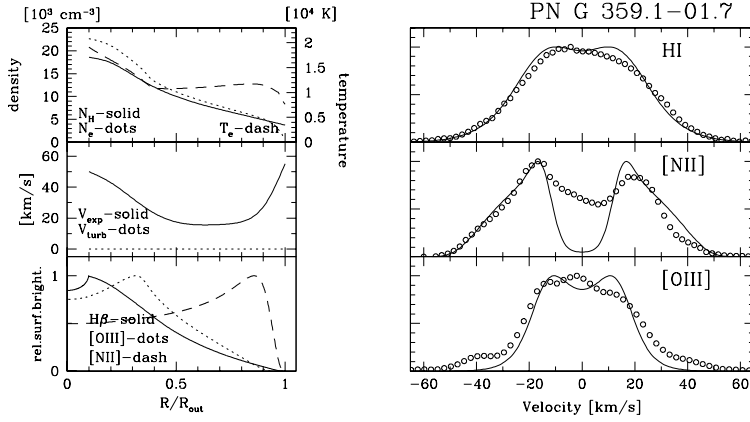


Fig. 13. As Fig. 1, for the PN 359.1-01.7

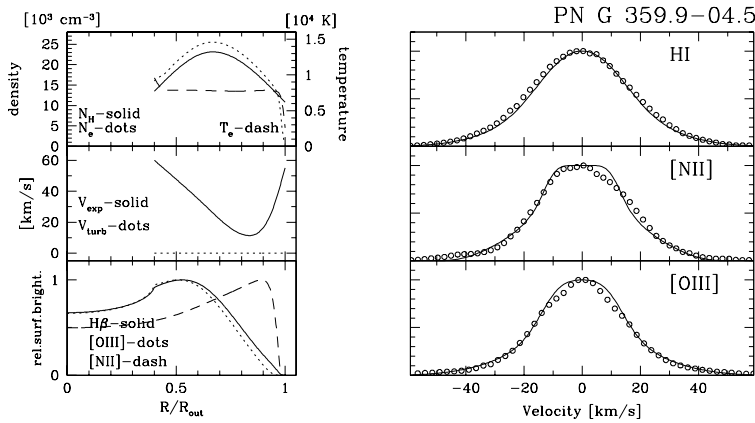


Fig. 14. As Fig. 1, for the PN 359.9-04.5

358.5–04.2 (*H I-46*) The radio image shows this to be a very compact PN (Acker et al. 1992). (The optical image appears to suffer from confusion with a nearby star: Bedding & Zijlstra 1994). A ‘U’-shaped velocity field was used. However, the narrow [O III] line is not well fitted. The H-line is also a little too narrow in the fit. Attempts to broaden this with a more complicated velocity field, without affecting the other lines, did not work.

359.1–01.7 (*M 1-29*) This is the most complicated object in the sample. The [O III] line shows several components including wings at extreme velocities and an unresolved component at the systemic velocity. The [N II] line shows far less splitting in the observed profile than in the fit. These facts suggest that a bipolar outflow exists in this object. The radio image confirms that this object is bipolar (Zijlstra et al. 1989). Thus, the extreme wings probably result from the polar flow, where the [O III] extends further into the nebula. The component at the systemic velocity could result from a near-stationary torus (but could also be due to the slit having been centered on the brightest component of the bipolar image). A very small inner radius of $0.1 \times R_{\text{out}}$ was used, with a density maximum at the inner edge. Such a structure is needed because of the lack of line splitting in the H α line, while the nebula is quite extended ($7''$). None of the lines are well fitted. A spherically symmetric model is probably a poor approximation to this nebula, and we

will not consider this object further. However, as the bipolarity was evident from the spectra, it appears likely that the other PNe in our sample do not show such complicated structures, even if good images are lacking.

359.9–04.5 (*M 2-27*) The image in Gathier et al. (1983) shows it to be almost unresolved. A ‘U’-shaped velocity gives a reasonable fit. There are some residuals in the line cores of [O III] and [N II].

4.2. Summary

Of the 14 objects studied, ‘U’-shaped velocity fields were required for 10. Of the remaining four, two show significant turbulence. Both nebulae contain [WC]-type central stars: turbulence around such stars appears to be common (Acker et al. 2002) although the origin of the turbulence is not clear (Mellema 2001). Three nebulae, including one of the turbulent objects, show monotonically increasing velocities. The prevalence of velocity maxima near the inner edge may be surprising. It was first found from the analysis of three PNe for which many emission line profiles were measured, in deep echelle spectra (Gesicki & Zijlstra 2003). The present result suggests inner acceleration may be quite common. In earlier papers we only looked at monotonic velocity fields. The larger residuals

Table 1. The expansion velocities and other data concerning the nebula and its central star. In column 8, the number in braces refers to the mass-averaged velocity found previously from fitting a single line only.

PN G	name	$\log T_{\text{eff}}$ [K]	$\log L$ [L_{\odot}]	dist. [kpc]	R_{out} [pc]	M_{ion} [M_{\odot}]	V_{av} [km s^{-1}]	remarks
002.6+08.1	H 1-11	4.81	3.4	7.0	0.1	0.21	19 (22)	wels
003.9-02.3	M 1-35	4.85	3.6	4.5	0.05	0.138	25 (26)	
006.1+08.3	M 1-20	4.90	3.4	6.0	0.026	0.045	12 (2)	
278.1-05.9	NGC 2867	5.08	3.1	2.0	0.07	0.15	28	[WO2]
278.8+04.9	PB 6	5.04	2.7	4.0	0.10	0.18	34	[WO1]
353.3+06.3	M 2-6	4.74	3.7	8.4	0.04	0.103	22 (22)	
353.5-04.9	H 1-36	5.08	3.5	7.0	0.03	0.061	32 (19)	
356.2-04.4	Cn 2-1	4.90	3.6	6.0	0.04	0.087	25 (23)	wels
357.1+03.6	M 3-7	4.85	3.0	4.0	0.05	0.074	19	wels
357.2+07.4	M 4-3	4.80	3.62	8.0	0.033	0.075	20 (18)	
358.2+03.6	M 3-10	4.97	3.0	5.0	0.04	0.048	27 (25)	
358.5-04.2	H 1-46	4.70	3.9	7.0	0.02	0.045	17 (5)	
359.1-01.7	M 1-29	5.08	3.5	3.0	0.05	0.128	24	bipolar
359.9-04.5	M 2-27	4.78	3.7	5.5	0.03	0.069	26 (26)	

in those fits may also be due to the presence of high-velocity gas near the inner edge.

The data show that the 14 PNe of our sample have on average high T_{eff} values, although within the usual temperature range. This is due to the high stellar temperature needed to obtain [O III] emission: at $T_{\text{eff}} < 410^4 \text{ K}$, this line is weak and these objects were not observed at the CAT. This selection effect should be taken into account when comparing the present 14 PNe with the larger sample, it is clearly visible in the figures discussed below, e.g. Fig. 19.

5. Discussion

5.1. Defining the expansion velocity

The earlier analysis using the [O III] line only assumed a linearly increasing velocity field. This often failed to fit the wings of the [O III] line, but a more complicated velocity field would be too poorly constrained. The present models show that most of the nebulae reveal a 'U'-shape velocity field. Whether this field is more common among PNe is hard to prove. Because of the selection effect described above, the U-shaped velocity field may be a consequence of a stronger wind blowing from the hotter stars in our sample.

We compute the mass-averaged expansion velocity V_{av} as described in Gesicki et al. (1998). This single value was introduced to characterize as simple as possible the nebular velocity field. These values are given in Table 1. In the same column in parentheses we show the V_{av} values obtained in Gesicki & Zijlstra (2000) from the [O III] line only with the assumption of a linear velocity field. It is found that the V_{av} do not differ much, except in two cases where previously we fitted the narrow line core only, neglecting the extended wings. We conclude that the mass averaged expansion velocity V_{av} is a well-defined parameter. Although its value is best derived using several spectral lines, a single line can give a reasonably good approximation to V_{av} , if the line shapes are not affected by perturbed veloc-

ity fields. It appears that the sharp increases of the expansion velocity towards the inner and outer nebular radius affect the line wings shapes but do not alter much the main flow. Very often the fit to the [N II] line wings requires a density decrease simultaneously with the increase of velocity; this reduced the impact of this region on V_{av} . The situation is less clear at the inner nebular radius, mostly because it is not well probed by the emission lines in our sample, but the smaller volume in this region contains a relatively small fraction of the nebular mass.

Our new data rather weaken the tendency found in Gesicki & Zijlstra (2000) that there seems to exist a weak correlation between the nebular outer radius and V_{av} . This is because the two lowest V_{av} values found in their paper are now revised upwards.

In the appendix we present a compilation of all PN for which expansion velocities have been determined. We note, however, that in most of these only monotonic velocity fields were considered. As argued above, especially the average expansion velocity (weighted by mass) appears to be relatively robust against such model simplifications. In the next subsections the large sample of 73 objects will be discussed. The smaller sample of 14 will be indicated in the figures.

5.2. The effect of metallicity

The thermal broadening of hydrogen amounts to roughly 15 km s^{-1} , which is similar to the typical expansion velocities. For this reason the hydrogen lines are not so sensitive to the details of the velocity fields and in previous papers have been relatively easy to fit. But here we find that the models which best reproduce O and N tend to fail at $\text{H}\alpha$, making the line either slightly too narrow or too broad.

This may suggest that our photoionization model produces incorrect electron temperatures, as this is the parameter which affects hydrogen but to which the other, heavier atoms are much less sensitive.

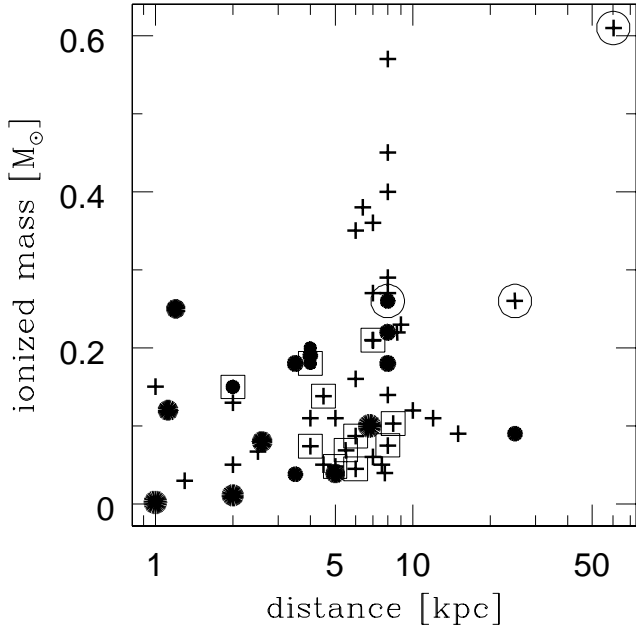


Fig. 15. Ionized nebular mass versus distance for the PNe. All analysed earlier PNe are shown. The [WC]-type PNe are presented as circles with their size proportional to their assigned [WC] class. Other PNe are presented as pluses. The objects analysed in the present article are framed with squares, and the three objects from Gesicki & Zijlstra (2003) are framed with circles. The distances are plotted in logarithmic scale to include the Sagittarius and SMC nebulae

The electron temperature is determined partly by the stellar temperature but most strongly by the metallicity. The reason is that most of the cooling of the nebula occurs from the forbidden oxygen lines. A lower abundance of oxygen leads to reduced cooling efficiency which is compensated by a higher electron temperature. We ran some test models, and found this to be the strongest effect in changing the width of the hydrogen line.

We did not attempt to perform our own chemical composition analysis.

5.3. Ionized masses

One of the results of photoionization modelling is the amount of ionized gas in the PN. This value is adopted to fit the observed and dereddened $\log F(\text{H}\beta)$ at the assumed distance, size and density distribution. It can be adjusted simultaneously with the distance which is often poorly known. Sometimes it is possible to build similarly satisfying models with different masses and distances: the selection is made based on additional data. In Fig. 15 we plot the derived ionized masses against the adopted distance. This figure shows that most of our PNe have ionized masses below $0.2 M_{\odot}$. The detailed analysis of Gesicki & Zijlstra (2003) of three PNe resulted in higher ionized masses than generally expected. This finding supports our earlier results of adopting higher masses for the Galactic Bulge nebulae. However it seems likely that some of our PNe can be shifted

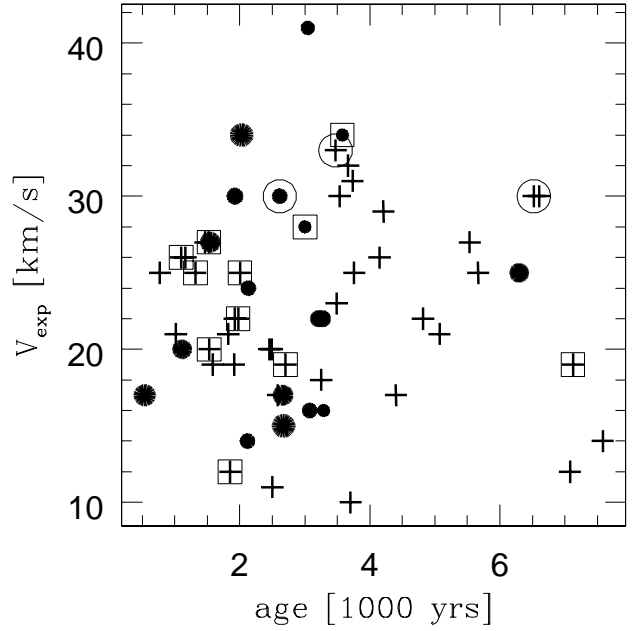


Fig. 16. Nebular mass-averaged expansion velocity plotted against dynamical age. All PNe with known metallicity are shown. The data are marked as in Fig. 15.

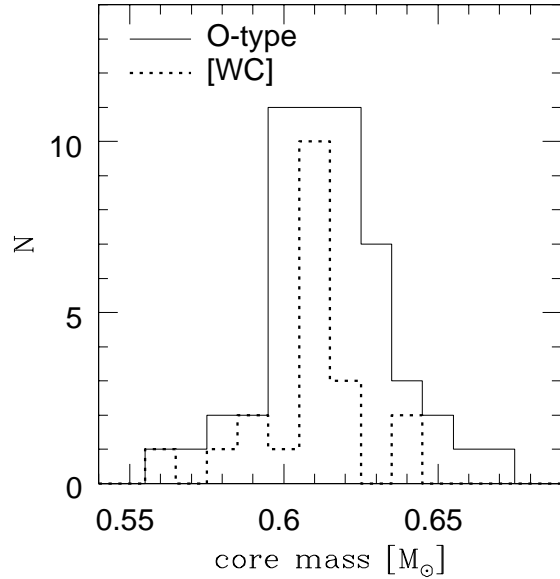


Fig. 17. Histogram of the nebular core masses. All analysed earlier PNe are included, the non-[WC] PNe (the solid line) and the [WC]-type PNe (the dotted line) are plotted separately.

between small distance & low mass and large distance & high mass regions in the plot.

5.4. Dynamical ages and core masses

The original AGB outflow velocity V_{AGB} can be estimated if the luminosity and metallicity of the star is known. Habing et al. (1994) show that $V_{\text{AGB}} \propto L_*^{0.33} \delta^{0.5}$ where δ is the dust-to-gas ratio, assumed to be proportional to metallicity. We have calculated (see Gesicki & Zijlstra 2000) V_{AGB} for the PNe with known metallicity (using the O/H in Table A.1). We assumed that a star with solar metallicity (O/H=8.93) has an AGB outflow velocity of 15 km s^{-1} .

Gesicki & Zijlstra (2000) describe a procedure to estimate the dynamical ages of the PNe and masses of their central stars. We follow their recipe for estimating the nebular dynamical age, by calculating the average of the PN expansion velocity and the original AGB velocity, and apply this value to a radius of 0.8 times the outer radius.

The mass-averaged expansion velocities we plot in Fig. 16 versus the dynamical age. We do not include objects for which the metallicity is not known. There is no apparent correlation which suggests that PNe do not speed up with time. Instead the increasing ionization flux together with increasing stellar wind are used for ionizing and accelerating more mass. The plot may suggest that [WC]-type PNe are younger than average PNe.

To find the stellar parameters we applied the computer codes to interpolate between the evolutionary tracks of Blöcker (1995) and Schönberner (1983). These codes were written by S.K. Górny and applied in Górny et al. (1997) for the derivation of PN core masses. The basic idea of these programmes is to produce by cubic spline interpolation a very dense grid of evolutionary tracks. We adopted these routines to extract for each stellar temperature, the luminosity and core mass against the evolutionary age. Then we interpolate the core mass and luminosity for each object, based on its dynamical age and stellar temperature. Because the dynamical age depends on the adopted AGB wind velocity, which value is depending on stellar luminosity, we performed a simple iteration. At first we adopted the luminosities found from photoionization modelling, then having located the objects on their evolutionary tracks we recalculated the AGB velocities with new luminosities and again interpolated stellar parameters.

The average core mass of the 14 PNe modelled in this paper is $0.62 M_{\odot}$. This is somewhat higher than the mean value obtained by Gesicki & Zijlstra (2000). This difference can be explained again by the previously mentioned selection effect, because more massive stars evolve faster and can reach higher temperatures before the surrounding nebula disperses.

For all PNe analyzed earlier we present the histograms of core masses in Fig. 17. Both the average and the median values are now $0.61 M_{\odot}$. Separately we give the histogram for O-type central stars and for those of [WC]-type. Both histograms look similar; however, the [WC]-type objects reveal a more pronounced peak at the central position. This finding needs verification on a bigger sample.

Although the *relative* core masses are well determined, including the narrow range in masses, the possibility of systematic effects cannot be excluded. We assume that the acceleration of the nebula occurred uniformly over time. If more time was spent at the original AGB velocity, the dynamical age

would be underestimated and the core mass overestimated. We can quantify this by repeating our calculation using the AGB wind velocity only, applied to the measured outer radius. This maximises the age and returns the lowest possible core mass. We find a systematic uncertainty due to this effect of about $-0.015 M_{\odot}$. This gives a *lower limit* to the mean core mass of about $0.6 M_{\odot}$. The definition of zero position on evolutionary timescale also introduces a systematic effect.

The evolutionary tracks are affected by the poorly known post-AGB mass-loss rates. The tracks assume a mass loss tapering off after the AGB, until replaced by a Pauldrach et al. (1988) wind. If the mass-loss rate becomes similar to the nuclear burning rate ($\sim 10^{-7} M_{\odot} \text{ yr}^{-1}$), the evolution in the HR diagram will accelerate and the same time scales will be reproduced for lower core masses. There is at present no evidence that mass-loss rates from central stars of planetary nebulae reach such high values. For the early post-AGB phase, the Blöcker (1995) tracks use much higher mass-loss rates than used by Vassiliadis & Wood (1993); the latter predicts much slower evolution which would give even higher core masses.

The peak of the mass distribution of white dwarfs in the solar neighbourhood is approximately $0.59 M_{\odot}$ (Napiwotzki et al. 1999). Although nominally discrepant, the difference can be due to systematic effects, especially the effect of mass loss on the post-AGB evolutionary tracks. The mass loss in the early post-AGB phase may be higher than assumed by Blöcker (1995), or significant mass loss event may happen during the PN evolution. The 'U'-shaped velocity fields for which we find evidence could be indicative of a strong wind during the PN phase, but it is not evident that this wind is massive enough to affect the speed of the stellar evolution.

5.5. Evidence for photon leakage

In Fig. 18 we plot for each object the ratio of the central star luminosity obtained from photoionization modelling over the dynamical luminosity obtained from timescales and evolutionary tracks interpolation. This ratio varies between 2 and 0.1, with the majority below 1. There is some indication that the mean ratio declines with increasing temperature. The values above unity probably reflect the uncertainty of the ionization models, which for instance are quite sensitive to the distance.

Calculating the core masses for the limiting case of no post-AGB acceleration, which gives lower luminosities, does not remove the discrepancy between the luminosities. Taking larger distances can bring the average values in agreement, but results in very large ionized masses. Also, about half our sample is in the Bulge and has well-determined (within 25%) distances.

The stellar luminosity obtained from our modelling is the one needed to ionize just the amount of mass needed to emit like the observed nebula. The fact that the model luminosity is smaller than the value predicted by evolutionary tracks may suggest that the nebula does not intercept and transform all stellar ionizing flux. In other words, the nebulae are leaking. This phenomenon seems to be stronger for the PNe whose cores evolved to higher temperatures. In the sample of 14 nebulae, only a single object is found to be density bounded. In the full

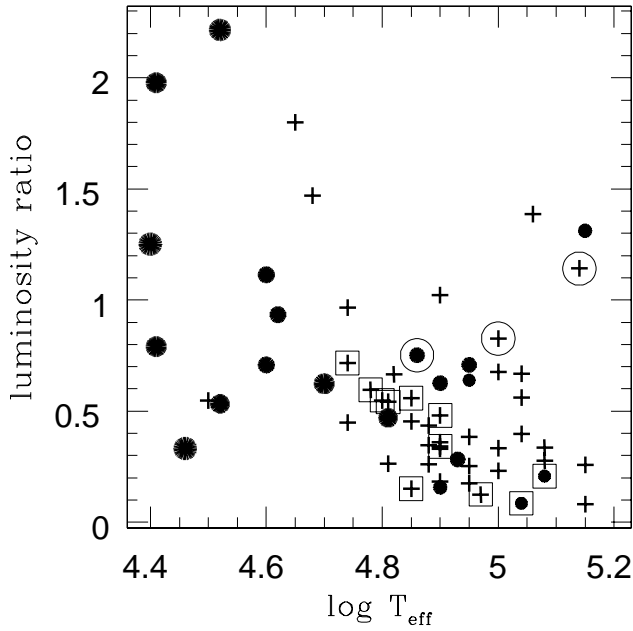


Fig. 18. The ratio between the stellar luminosity obtained from photoionization modelling and the one obtained from evolutionary tracks interpolation. The data are marked as in Fig. 15.

sample, few nebulae are density bounded. The other objects are ionization bounded and are not expected to 'leak' under the assumption of spherical symmetry. The evidence for leaks points to asymmetries, or clumping.

5.6. The objects on the HR diagram

The procedure used in calculating the core masses also returns the luminosity of the central star. Together with the central star effective temperatures obtained from the photoionization models, we can plot the PNe in a 'dynamical' HR diagram. Fig. 19 combines all objects from our earlier publications, the PNe analysed in this paper (framed with squares), and the three PNe of Gesicki & Zijlstra (2003) (framed with circles). Because we have two estimations of stellar luminosities we present the data in two boxes.

The objects show a strong clustering around a single evolutionary track. The fact that the objects agree fairly well with a single track across a range of temperatures suggests that the relative speed of evolution of the tracks is probably correct. If, for instance, the evolution would speed up at a certain temperature, this would appear as a tilted observed sequence compared to the theoretical tracks. Such a tilt is not evident.

We have no objects on the cooling track. The knee in the HR diagram is traversed very quickly (Blöcker 1995) so that few objects would be expected there. Further down on the cooling track the PN become very faint. However, near the knee the procedure to determine the mass and luminosity as a function of temperature and age has two solutions. We select the more luminous one and therefore may have missed one or more objects on the cooling track. The luminosity independently determined in the ionization model provides a check: in only one

case (M2-11, a Bulge PN) could this place the object low on the cooling track.

The lower panel of Fig. 19 shows the same diagram but now using the luminosity from the photoionization model. Comparing the two panels shows that the model luminosities do not cluster in the diagram, and are almost always lower than the dynamical luminosities. The lower panel also shows a characteristic decline of luminosity with increasing temperature, in contradiction to the horizontal tracks. This decline has often been seen in nebular luminosities, e.g. Pottasch (1984). Comparison with the dynamical luminosities suggest that measurements of the nebulae (e.g., using the relation $L_* = 150L_{\text{H}\beta}$, Gathier & Pottasch 1989, Zijlstra & Pottasch 1989, Magrini et al. 2002), especially with hotter stars, underestimate the stellar luminosity.

5.7. [WC]-type planetary nebulae

In all figures of section 5 we separated the [WC]-type PNe from other types to check how this group of objects behaves. These PNe are characterised by the presence of a hydrogen-deficient central star, which has a much stronger (10–100 times) stellar wind than other PNe cores. Approximately 8% of PNe have [WC]-type stars (Górny 2001). The nebulae surrounding [WC]-type and O-type stars are, however, very similar. The work of Gesicki & Acker (1996) and Acker et al. (2002) discusses a significant difference between the complete two groups: [WC]-type PNe are characterised by strong turbulent motions while the other are not.

Our present work confirms the limited observable differences concerning the turbulent motions. The distribution of stellar temperatures is different, with the [WC] stars being on average some 20 000 K cooler—they dominate our sample at the coolest temperatures. However, they were taken from a different sample and this difference can be explained by selection effects. Otherwise, the expansion velocities, ionized masses, the histogram of derived central star masses and the distribution in the HR diagram are the same between the [WC] and non-[WC] stars. From the presented HR diagram it looks very likely that the [WC]-type stars follow the same evolutionary tracks as the other PNe, and are derived from the same progenitor population.

The fact that turbulence is an exclusive property of [WC] stars shows that evolution from [WC] star to non-[WC] star must be rare at best, and that the known [WC] stars spend a sufficient amount of time in this phase for their winds to impart sufficient kinetic energy to the nebulae to cause the observed turbulence. The nebular ages are also no different between [WC] and non-[WC] stars. All these factors suggest that although the two groups arise from the same stellar population, the [WC] stars separate relatively early in the post-AGB evolution. The model where the strong wind strips the hydrogen layer of a helium burning star can explain the observed correlation between [WC] stars and turbulence, as well as the otherwise very similar nebulae.

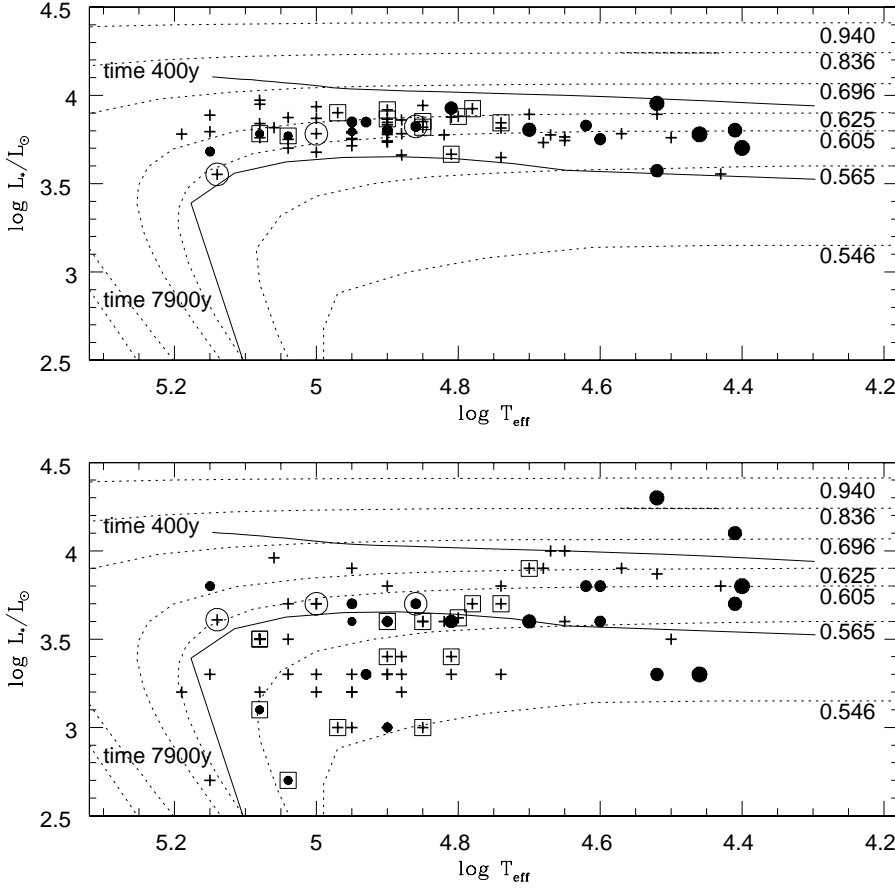


Fig. 19. HR diagram for the PNe. All PNe analysed earlier are included. The objects are marked as in Fig. 15. The upper panel corresponds to the dynamical luminosities, the lower to the photoionization model luminosities (see text). The evolutionary tracks are overplot (dotted lines, labelled with core mass values), also are shown the lines corresponding to the smallest and the largest dynamical age of presented sample

6. Conclusions

We have presented the expansion velocity fields in a sample of 14 planetary nebulae. The nebulae have high resolution spectra covering for each object three emission lines probing different nebular layers.

Two PNe show significant turbulence and both contain [WC]-type central stars. This confirms the existing evidence that turbulence around such stars is common (Acker et al. 2002).

Three nebulae, including one of the turbulent objects, show monotonically increasing velocities.

For ten objects (nonturbulent) we derived a U-shaped velocity field. The outer velocity increase is a well-understood feature of the ionization front. The inner velocity increase was postulated recently by Gesicki & Zijlstra (2003) for two PNe with very hot cores (above 100 000 K). We explained this in terms of a strong wind blowing from a hot central star and sweeping up the inner nebular layers. We thought of it as an exception but the presented results suggests that the inner acceleration may be quite common. It is already present at $T_{\text{eff}} \sim 50000$ K which is the lowest value in our sample.

We found that the mass-averaged expansion velocity is a reasonably robust parameter. It is well determined even from a

single emission line, if this line doesn't exhibit unusual features. The recently derived U-shape velocity fields result in much improved fits to the line wings, but the V_{av} are almost the same as obtained with simple linearly increasing velocity. We conclude that V_{av} is the proper parameter to describe the main nebular flow.

In the discussion we assembled all previously analysed nebulae. This has not been done before. 24 objects have been discussed by Acker et al. (2002); those PNe were observed in three or more emission lines. 44 objects have been discussed by Gesicki & Zijlstra (2000), observed only in the [O III] 5007Å line. Because we find that the mass-averaged expansion velocity is a robust parameter, we decided to merge the two samples and add three PNe from Gesicki & Zijlstra (2003).

Applying the interpolation routines for evolutionary tracks, we estimate the nebular core masses. The values for our sample of 14 are somewhat larger than the mean value for the full sample. The mean value for the whole sample of 73 PNe is $0.61 M_{\odot}$ which is higher than the expected average white dwarf mass. This difference can possibly be explained in terms of systematic effects.

For all discussed PNe we also interpolated the predicted by evolutionary calculation stellar luminosities. We find that for

the 14 PNe and for the majority of the remaining nebulae, our stellar luminosities are higher than the values obtained from the photo-ionization model of the nebula. We conclude that PNe do not intercept all ionizing radiation even when there is strong evidence of the presence of an ionization boundary.

All analysed PNe show a strong clustering around a single evolutionary track on the HR diagram. This provides support for the evolutionary calculations.

In the discussion we separated the [WC]-type PNe from other types. In all plots presented the distributions of the two groups are actually the same. It looks like the [WC]-type stars follow the same evolutionary track as the other PNe cores. However, their true position on the HR diagram may be masked by pseudo-photospheres in the strong wind.

Acknowledgements

The evolutionary tracks interpolation routines were kindly provided by S.K.Górny. This project was financially supported by the CNRS through the JUMELAGE “Astronomie Pologne” programme, by the “Polish State Committee for Scientific Research” through the grant No. 2.P03D.020.17 and by a PPARC visitor grant PPA/G/O/2001/00483.

References

- Aaquist O.B., Kwok S., 1990, *A&AS* 84, 229
 Acker A., Ochsenbein F., Stenholm B., et al., 1992, Strasbourg – ESO Catalogue of Galactic Planetary Nebulae. ESO, Garching (CGPN)
 Acker A., Gesicki K., Grosdidier Y., Durand S., 2002, *A&A* 384, 620
 Bedding T.R., Zijlstra A.A., 1994, *A&A* 283, 955
 Blöcker T., 1995, *A&A* 299, 755
 Gathier R., Pottasch S. R., Goss W. M., van Gorkom J. H., 1983, *A&A* 128, 325
 Gathier R., Pottasch S. R., 1989, *A&A* 209, 369
 Gesicki K., Acker A., 1996, *Ap&SS* 238, 101
 Gesicki K., Acker A., Szczerba R., 1996, *A&A* 309, 907
 Gesicki K., Zijlstra A.A., Acker A., Szczerba R., 1998, *A&A* 329, 265
 Gesicki K., Zijlstra A.A., 2000, *A&A* 358, 1058
 Gesicki K., Zijlstra A.A., 2003, *MNRAS* 338, 347
 Górny S., 2001, *ApSS* 275, 67
 Górny S.K., Stasińska G., Tyłenda R., 1997, *A&A* 318, 256
 Habing H.J., Tignon J., Tielens A.G.G.M., 1994, *A&A* 286, 523
 Magrini L., Corradi R. L. M., Walton N. A., et al., 2002, *A&A* 386, 869
 Mellema G., 2001, *ApSS* 275, 147
 Napiwotzki R., Green P.J., Saffer R.A., 1999, *ApJ* 517, 399
 Pauldrach A., Puls J., Kudritzki R.P., et al., 1988, *A&A* 207, 123
 Peña M., Stasińska G., Medina S., 2001, *A&A* 367, 983
 Pottasch S.R., 1984, “Planetary Nebulae”, D.Reidel Publishing Company, Dordrecht, Holland
 Richer H.B., Fahlman G.G., Ibata R.A., et al., 1997, *ApJ*, 484, 741
 Schönberner D., 1983, *ApJ*, 272, 708
 Schwarz H.E., Corradi R.L.M., Melnick J., 1992, *A&AS* 96, 23
 Stasińska G., Tyłenda R., 1994, *A&A*, 289, 225
 Vassiliadis E., Wood P.R., 1993, *ApJ* 413, 641
 Zijlstra A.A., 1999, in: *Asymptotic Giant Branch Stars* (edited by C. Waelkens), p.555
 Zijlstra A.A., Pottasch S.R., Bignell C., 1989, *A&AS* 79, 329
 Zijlstra A.A., Pottasch S.R., 1989, *A&A*, 216, 245

Appendix A: Full sample of mass-averaged expansion velocities

We present here the data concerning the full sample of PNe with mass-averaged expansion velocities derived. The table contains in consecutive columns: the PNG designation, the usual name, stellar effective temperature, stellar luminosity derived from photoionization models, assumed distance, physical outer radius, model’s ionized mass, mass-averaged expansion velocity, additional turbulent velocity, O/H abundance ratio, nebular dynamical age, interpolated central star mass, remarks.

Table A.1. The expansion velocities and other data concerning the nebula and its central star. Part 1.

PNG	name	$\log T_{\text{eff}}$ [K]	$\log L$ [L_{\odot}]	dist. [kpc]	R_{out} [pc]	M_{ion} [M_{\odot}]	V_{av} [km s^{-1}]	V_{turb} [km s^{-1}]	O/H	t_{dyn} [10^3y]	M_* [M_{\odot}]	remarks
001.5-06.7	SwSt1	4.52	4.30	2.00	0.007	0.011	17.0	14	7.50	0.53	0.640	WC10
001.7-04.6	H1-56	4.95	3.00	10.0	0.08	0.12	17.0	0	8.73	4.40	0.606	
002.0-06.2	M2-33	4.74	3.30	8.00	0.10	0.27	12.0	0	8.69	7.07	0.574	
002.0-13.4	IC4776	4.60	3.60	3.50	0.06	0.18	22.0	0	8.25	3.27	0.594	WC6
002.1-02.2	M3-20	4.88	3.20	7.00	0.10	0.27	32.0	0	8.64	3.66	0.607	
002.6+08.1	H1-11	4.81	3.40	7.00	0.10	0.21	19.0	0	7.60	7.12	0.579	
003.1+02.9	Hb4	4.95	3.6	4.0	0.065	0.2	16.0	14	8.92	3.28	0.612	WC3
003.2-06.2	M2-36	4.90	3.30	6.40	0.11	0.38	22.0	0	8.89	4.81	0.601	
003.7-04.6	M2-30	5.04	3.50	7.00	0.10	0.36	26.0	0	8.74	4.15	0.610	
003.8-17.1	Hb8	4.88	3.40	15.0	0.04	0.09	22.0	0	8.58	1.92	0.622	
003.9-02.3	M1-35	4.85	3.60	4.50	0.05	0.138	25.0	0	8.83	2.00	0.619	
004.0-03.0	M2-29	4.88	3.30	9.00	0.08	0.23	14.0	0	7.46	7.58	0.581	
004.2-04.3	H1-60	4.90	3.00	7.00	0.10	0.21	21.0	0	8.61	5.07	0.599	WC?
004.8-22.7	He2-436	4.95	3.70	25.0	0.03	0.09	14.0	0	8.36	2.11	0.622	WC5
004.9+04.9	M1-25	4.62	3.8	8.0	0.06	0.18	30.0	12	9.09	1.92	0.611	WC6
005.2+05.6	M3-12	5.0	3.2	8.0	0.15	0.57	30.0	0	8.14	6.60	0.595	
005.8-06.1	NGC6620	5.04	3.3	8.0	0.14	0.45	27.0	0	8.84	5.53	0.603	
006.0-03.6	M2-31	4.86	3.7	8.00	0.07	0.26	30.0	0	8.7	2.61	0.614	wels
006.1+08.3	M1-20	4.90	3.40	6.00	0.026	0.045	12.0	0	8.53	1.85	0.624	
006.8-19.8	Wray16-423	5.00	3.70	25.0	0.09	0.26	33.0	0	8.33	3.47	0.613	wels
006.8+04.1	M3-15	4.90	3.6	4.0	0.06	0.19	16.0	15	8.89	3.07	0.612	WC4-6
008.3-01.1	M1-40	5.15	3.3	2.5	0.042	0.067	27.0	0	9.02	1.46	0.648	
009.4-09.8	M3-32	4.95	3.20	7.00	0.10	0.26	23.0	0	0	4.53	0.605	
009.6-10.6	M3-33	4.95	3.30	8.00	0.12	0.40	25.0	0	8.45	5.66	0.598	
010.7-06.4	IC4732	4.82	3.60	8.00	0.08	0.29	25.0	0	8.42	3.75	0.604	
027.6+04.2	M2-43	4.81	3.6	5.0	0.02	0.039	20.0	10	8.30	1.11	0.636	WC8
029.2-05.9	NGC6751	4.90	3.0	2.0	0.1	0.15	41.0	15	8.60	3.04	0.612	WC4
064.7+05.0	BD+30	4.41	4.1	2.6	0.035	0.08	27.0	15	8.40	1.54	0.606	WC9
096.4+29.9	NGC6543	4.70	3.6	1.12	0.05	0.12	17.0	12	8.75	2.66	0.608	WC9
120.0+09.8	NGC40	4.52	3.3	1.2	0.14	0.25	25.0	8	8.70	6.29	0.564	WC8
123.6+34.5	IC3568	4.68	3.9	2.0	0.1	0.13	29.0	0	8.43	4.20	0.590	O3(H)
144.5+06.5	NGC1501	5.15	3.8	1.2	0.16	0.18	40.0	10	0	4.17	0.614	WC4
146.7+07.6	M4-18	4.4	3.8	6.8	0.06	0.1	15.0	15	9.23	2.67	0.580	WC11
215.2-24.2	IC418	4.57	3.9	1.0	0.036	0.05	15.0	0	0	2.50	0.602	Of(H)
221.3-12.3	IC2165	5.19	3.2	2.5	0.057	0.076	25.0	14	0	2.37	0.632	wels?
261.0+32.0	NGC3242	4.9	3.3	1.0	0.1	0.15	31.0	0	8.66	3.73	0.608	O(H)
278.1-05.9	NGC2867	5.08	3.1	2.0	0.07	0.15	28.0	12	8.44	3.00	0.619	[WO2]
278.8+04.9	PB6	5.04	2.7	4.0	0.1	0.18	34.0	16	8.57	3.57	0.614	[WO1]

Table A.2. The expansion velocities and other data concerning the nebula and its central star. Part 2.

PNG	name	$\log T_{\text{eff}}$ [K]	$\log L$ [L_{\odot}]	dist. [kpc]	R_{out} [pc]	M_{ion} [M_{\odot}]	V_{av} [km s^{-1}]	V_{turb} [km s^{-1}]	O/H	t_{dyn} [10^3y]	M_* [M_{\odot}]	remarks
285.4+01.5	Pe1-1	4.93	3.3	3.5	0.05	0.038	24.0	10	8.75	2.13	0.621	WC4-5
296.3-03.0	He2-73	5.00	3.70	4.00	0.04	0.11	19.0	0	8.80	1.91	0.629	
307.2-09.0	He2-97	4.81	3.30	4.50	0.03	0.05	19.0	0	8.58	1.58	0.624	
327.1-02.2	He2-142	4.41	3.7	3.5	0.03	0.03	20.0	7	0	1.56	0.605	WC9
327.5+13.3	He2-118	4.90	3.00	7.00	0.03	0.03	13.0	0	0	2.40	0.617	
345.0-04.9	Cn1-3	4.65	3.60	7.50	0.05	0.12	16.0	0	0	3.25	0.598	
345.2-08.8	Tc1	4.5	3.5	2.0	0.05	0.05	20.0	0	8.71	2.49	0.596	Of(H)
346.3-06.8	Fg2	5.08	3.20	8.70	0.10	0.22	30.0	0	8.91	3.53	0.615	
347.4+05.8	H1-2	5.06	3.96	7.00	0.03	0.10	11.0	0	8.33	2.49	0.623	
349.8+04.4	M2-4	4.74	3.80	6.00	0.05	0.16	17.0	0	8.80	2.58	0.610	
350.9+04.4	H2-1	4.52	3.87	5.00	0.03	0.06	36.0	0	0	0.86	0.624	
351.9+09.0	PC13	4.95	3.90	6.00	0.10	0.15	29.0	0	0	3.59	0.610	
352.9-07.5	Fg3	4.67	4.00	7.00	0.03	0.09	10.0	0	0	3.12	0.601	
352.9+11.4	K2-16	4.46	3.3	1.0	0.05	0.002	34.0	12	7.90	2.02	0.600	WC11
353.3+06.3	M2-6	4.74	3.70	8.40	0.04	0.103	22.0	0	8.51	1.97	0.615	
353.5-04.9	H1-36	5.08	3.50	7.00	0.03	0.061	32.0	0	0	0.97	0.659	
355.1-02.9	H1-31	5.04	3.70	12.0	0.04	0.11	21.0	0	8.77	1.82	0.633	
355.1-06.9	M3-21	4.95	3.20	5.00	0.06	0.11	18.0	0	8.65	3.25	0.613	
355.4-02.4	M3-14	4.90	3.80	6.00	0.08	0.35	23.0	0	8.79	3.48	0.609	
355.7-03.5	H1-35	4.65	4.00	8.00	0.04	0.14	10.0	0	8.27	3.70	0.593	
355.9-04.2	M1-30	4.60	3.8	8.00	0.07	0.22	22.0	0	8.76	3.21	0.594	wels
356.2-04.4	Cn2-1	4.90	3.60	6.00	0.04	0.087	25.0	0	9.20	1.31	0.636	
356.9+04.5	M2-11	5.15	2.70	7.00	0.05	0.06	20.0	0	8.75	2.45	0.628	
357.1+03.6	M3-7	4.85	3.0	4.0	0.05	0.074	19	0	8.56	2.70	0.613	
357.2+07.4	M4-3	4.80	3.62	8.00	0.033	0.075	20.0	0	8.79	1.53	0.624	
358.2+03.6	M3-10	4.97	3.00	5.00	0.04	0.048	27.0	0	8.81	1.52	0.635	
358.5-04.2	H1-46	4.70	3.90	7.00	0.02	0.045	17.0	0	0	1.22	0.625	
358.7-05.2	M3-40	5.00	3.30	7.60	0.03	0.05	26.0	0	8.80	1.16	0.647	
359.1-01.7	M1-29	5.08	3.5	3.0	0.05	0.128	24.0	0	0	2.17	0.629	bipolar
359.2-33.5	CRBB1	4.43	3.8	3.5	0.08	0.18	13.0	0	0	6.41	0.562	O(H)
359.3-00.9	Hb5	5.08	3.50	1.30	0.02	0.03	25.0	0	8.84	0.77	0.668	
359.7-02.6	H1-40	4.85	3.60	7.80	0.02	0.04	21.0	0	8.45	1.01	0.642	
359.8-07.2	M2-32	4.90	3.60	7.00	0.06	0.19	29.0	0	0	2.15	0.620	
	SMP5	5.14	3.61	60.3	0.15	0.61	30.0	0	8.28	6.52	0.604	
359.9-04.5	M2-27	4.78	3.70	5.50	0.03	0.069	26.0	0	8.93	1.10	0.634	